GRAPHENE

Measuring Hall viscosity of graphene's electron fluid

A. I. Berdyugin[1]*, S. G. Xu[1,2]*, F. M. D. Pellegrino[3,4], R. Krishna Kumar[1,2], A. Principi[1], I. Torre[5], M. Ben Shalom[1,2], T. Taniguchi[6], K. Watanabe[6], I. V. Grigorieva[1], M. Polini[7,1], A. K. Geim[1,2]†, D. A. Bandurin[1]†

An electrical conductor subjected to a magnetic field exhibits the Hall effect in the presence of current flow. Here, we report a qualitative deviation from the standard behavior in electron systems with high viscosity. We found that the viscous electron fluid in graphene responds to nonquantizing magnetic fields by producing an electric field opposite to that generated by the ordinary Hall effect. The viscous contribution is substantial and identified by studying local voltages that arise in the vicinity of current-injecting contacts. We analyzed the anomaly over a wide range of temperatures and carrier densities and extracted the Hall viscosity, a dissipationless transport coefficient that was long identified theoretically but remained elusive in experiments.

Electron transport in metallic systems is routinely described in terms of classical charges that whizz through the bulk and scatter at various defects, such as impurities, edges, or lattice vibrations. This semiclassical picture does not hold, however, for materials in which defects are scarce, and electron-electron collisions provide the shortest scattering length. In the latter case, electrons respond to external fields collectively so that their transport resembles a classical fluid flow (*1*–*3*). The studies of electron hydrodynamics have been hampered by the scarcity of experimental systems in which both impurity and electron-phonon scattering—which do not conserve the electron momentum—are weak so that electron-electron collisions become the dominant source of scattering. The situation has changed recently owing to improvements in materials quality (*4*, *5*), including high-quality graphene with its exceptionally weak electron-phonon coupling (*6*–*8*). Transport experiments have provided clear evidence for a fluid-like behavior of charge carriers in graphene, which reveals itself in, for example, negative vicinity resistance (*6*, *7*) and superballistic transport (*8*). Good agreement between the experiments and theory indicates that electron transport in high-quality graphene at temperatures (T) above 100 K is consistent with the hydrodynamics description (*7*, *9*–*13*).

[1]School of Physics and Astronomy, University of Manchester, Manchester M13 9PL, UK. [2]National Graphene Institute, University of Manchester, Manchester M13 9PL, UK. [3]Dipartimento di Fisica e Astronomia, Università di Catania, Via S. Sofia, 64, I-95123 Catania, Italy. [4]Istituto Nazionale di Fisica Nucleare, Sez. Catania, I-95123 Catania, Italy. [5]ICFO–Institut de Ciències Fotòniques, Barcelona Institute of Science and Technology, 08860 Castelldefels (Barcelona), Spain. [6]National Institute for Materials Science, 1-1 Namiki, Tsukuba, 305-0044 Japan. [7]Istituto Italiano di Tecnologia, Graphene Labs, Via Morego 30, 16163 Genova, Italy.
*These authors contributed equally to this work.
†Corresponding author. Email: geim@manchester.ac.uk (A.K.G.); bandurin.d@gmail.com (D.A.B.)

So far, studies of electron hydrodynamics focused on zero magnetic field B. On the other hand, the finite B regime described by a combination of the Navier-Stokes and Maxwell's equations is relevant for many research fields, ranging from astrophysics to plasma physics to geophysics and engineering. For static B, the viscous response of a charged fluid is described by a tensor in the Navier-Stokes equation that contains a dissipationless, off-diagonal coefficient called Hall or odd viscosity ν_H (*14*–*17*). To get some qualitative insight into the behavior of a two-dimensional (2D) electron fluid subjected to a nonquantizing magnetic field, we plotted the calculated electric potential distribution $\phi(\boldsymbol{r})$ expected near a narrow current injector in zero (Fig. 1A) and finite B (Fig. 1B). The injected current I entrains adjacent fluid regions, which results in negative lobes of the potential near the injector (*18*, *19*). In zero B (Fig. 1A), the lobes are symmetric with respect to the injection direction and, for restricted geometries, can be accompanied by whirlpools of electric current (*18*–*22*). Finite B induces considerable asymmetry in $\phi(\boldsymbol{r})$ (Fig. 1B), which involves the following three contributions. First, the ordinary Hall effect (HE) causes the well-known potential difference $V_H = IB/ne$ between the left and right sides of the half-plane (Fig. 1C), where n is the carrier density and e is the elementary charge. The second contribution comes from the longitudinal viscosity $\nu(B)$ and, in small B, is practically indistinguishable from that shown in Fig. 1A for zero B. The third contribution arises from Hall viscosity, the main subject of our interest here. The ν_H contribution (Fig. 1D) is opposite in sign to the classical HE (Fig. 1C); ν_H suppresses the normal Hall response, but this influence rapidly decays away from the injector region (Fig. 1D). The latter feature makes it difficult to observe the Hall viscosity by using conventional devices and measurement geometries such as the standard Hall bar configuration (*15*, *16*). As shown below, the vicinity geometry (Fig. 1E) allows us to distinguish between the ordinary HE and the anomalous one caused by ν_H.

Our devices were multiterminal Hall bars such as shown in Fig. 1E and fig. S1, A and B. They were made from graphene encapsulated between hexagonal boron-nitride crystals (*22*). The Hall bars had typical widths of 2 to 4 μm and were endowed with narrow (~0.3 μm) and closely spaced (~0.5 μm) voltage probes (Fig. 1E). Such submicrometer probes are essential for detection of viscous effects as seen from the spatial scale of Fig. 1, A to D. Several devices made from mono- and bilayer graphene (MLG and BLG, respectively) were studied, all exhibiting similar behavior. The data reported below are from three MLG and two BLG devices that were studied in great detail. They had typical mobilities exceeding ~100,000 $cm^2 V^{-1} s^{-1}$ at all temperature (T) up to 300 K (*22*), which ensured micrometer-scale transport with respect to momentum-nonconserving scattering over the entire T range explored in the experiments (fig. S1); for comparison, the electron-electron mean free path at representative $n = 10^{12}$ cm^{-2} and $T = 150$ K is ~0.4 μm, shorter than a typical distance of ~1 μm, at which the viscous contribution was probed (*8*, *11*).

In the vicinity geometry, the current I was injected through a narrow contact (for example, Fig. 1E, probe 1) into a wide graphene channel, and the local potential ϕ was measured by using probe 3 positioned at the distance L from the injector. Contacts 2 and 4 (chosen sufficiently far away from the injection region) complete the electric circuit, serving as the drain and reference-voltage contacts, respectively. The vicinity resistance is defined as $R_v = R_{34,12} = V_{34}/I_{12}$, where V_{34} is the voltage drop between 3 and 4. As per Fig. 1, A to D, R_v is expected to be sensitive to viscous effects (*6*, *7*, *18*, *22*). According to the previous experiments and theory (*6*, *7*, *12*, *18*), R_v is a nonmonotonic function of T so that R_v is positive in the ballistic regime at low T, changes its sign to negative with increasing T, passes through a minimum, and then starts growing. The negative sign of R_v is a clear indicator that electron-electron scattering strongly affects ballistic transport (*6*, *7*, *12*, *18*, *22*), whereas the turning point marks the onset of the regime in which the hydrodynamics approach becomes applicable (*6*, *7*).

For the purpose of this Report, we focus on the latter regime, which in our devices starts above 100 to 150 K, depending on n (fig. S2A). In addition, we set several other constraints on variables used in the experiments. First, we limited ourselves to $B < 40$ mT so that the cyclotron radius always exceeded our devices' width. This was to avoid hydrodynamics effects being obscured by those caused by Landau quantization and electron focusing (*23*). In addition, such small B are not expected to affect the longitudinal viscosity ν. Second, to avoid unrelated effects

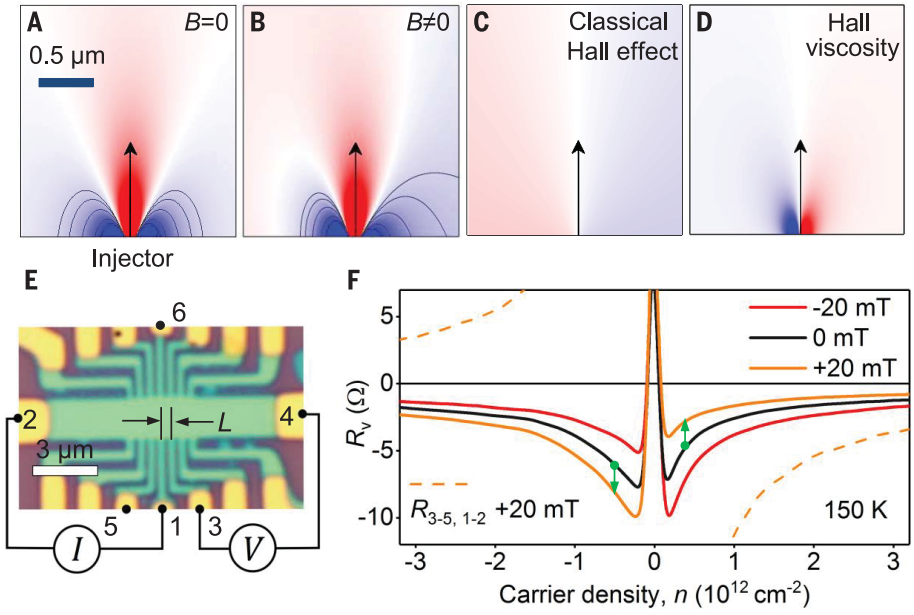

Fig. 1. Effect of magnetic field on viscous electron flow. (**A** and **B**) Electric potential distribution $\phi(\boldsymbol{r})$ expected in graphene's electron fluid near a current injector in zero B and 50 mT, respectively. The calculations were based on equations C15 and C16 of (*16*) by using characteristic zero-field viscosity $\nu_0 = 0.1$ m^2/s, found in our experiments; $n = 2 \times 10^{12}$ cm^{-2}; and $\tau = 2$ ps. Solid curves indicate equipotentials. (**C**) Contribution from the ordinary HE toward the map in (B). (**D**) Contribution that comes from ν_H. Color scale in (A) to (D) is dark blue to dark red and reflects −2.5 to +2.5 of the potential induced by the ordinary HE in (C). (**E**) Optical micrograph of one of our devices, along with the schematic of the vicinity geometry from which R_v is obtained. (**F**) Examples of the vicinity resistance for different B (solid curves); $L \approx 1$ μm. Dashed lines indicate Local Hall resistance measured by using voltage probes 3 and 5 close to the current injector (*22*).

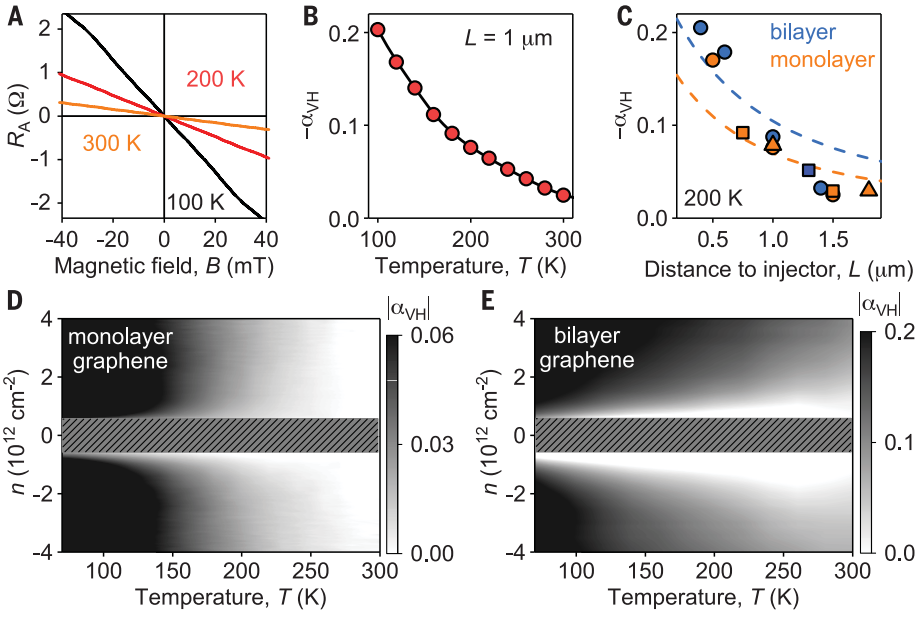

Fig. 2. Viscous Hall effect. (**A**) $R_A(B)$ for one of our MLG devices at $L \approx 1$ μm for three different temperatures. (**B**) The dimensionless viscous coefficient $\alpha_{VH}(T)$ (symbols). Reproducibility is provided in fig. S2C. (**C**) $\alpha_{VH}(L)$ found for five different devices indicated with different symbols, whereas the color refers to MLG and BLG. $n = 2 \times 10^{12}$ cm^{-2} for (A) to (C), which corresponds to the Fermi energy of ~165 and ~70 meV for MLG and BLG, respectively. Dashed lines in (C) indicate dependences from Eq. 2 with no fitting parameters; $\sigma_0(T)$ is determined as described in (*22*), section 1, and $\nu_0(T)$ is taken from experiment (*6*). (**D** and **E**) Maps of $|\alpha_{VH}|$ in MLG and BLG devices for $L \approx 1.5$ μm and 0.7 μm, respectively; $B = 40$ mT. Shaded areas indicate omitted analysis because the cyclotron diameter becomes comparable with the device width (*23*).

stemming from thermal excitations and charge inhomogeneity, we carried out experiments away from the charge neutrality point, at n of the order of 10^{12} cm^{-2}. Last, we used small $I \leq 1$ μA so as to stay in the linear response regime and avoid nonlinear effects, including electron heating (*2*, *6*).

Examples of $R_v(n)$ in the hydrodynamic regime are shown in Fig. 1F for one of our MLG devices. In agreement with the previous studies (*6*, *7*), R_v in zero B is negative for all n away from the charge neutrality and is practically symmetric for electron and hole doping (positive and negative n, respectively). The small positive field of 20 mT shifts the R_v curves in opposite directions for electrons and holes, as indicated by the green arrows in Fig. 1F. The shifts are opposite for negative B. This behavior implies a contribution that is antisymmetric with respect to B and n, similar to the ordinary HE. However, the latter cannot possibly explain the observed shifts because in the vicinity, geometry voltage probes are placed on the same side of the current path, which cancels the ordinary HE contribution to the measured voltages. A formal proof of this can be found in (*16*). Experimentally, we have also checked that there is no ordinary HE contribution for the vicinity geometry by using similar graphene devices but exhibiting low mobility (fig. S2, D to F). Furthermore, it is important to compare the sign of the R_v changes induced by B with the sign of the ordinary HE. To keep the same sign convention for B and n, it is instructive to measure the local Hall resistance $R_{35,12}$ (Fig. 1E and fig. S6) instead of using the standard Hall geometry. In this case, we used contact 5 instead of 4 and kept all the other contacts same as in the R_v measurements. This swap placed the voltage probes at the opposite sides of the current path, which gave rise to the voltage drop V_H owing to the ordinary HE. The antisymmetric-in-B part of $R_{35,12}$ (to avoid a contribution from longitudinal resistivity) is plotted in Fig. 1F (dashed lines). It shows that the ordinary HE

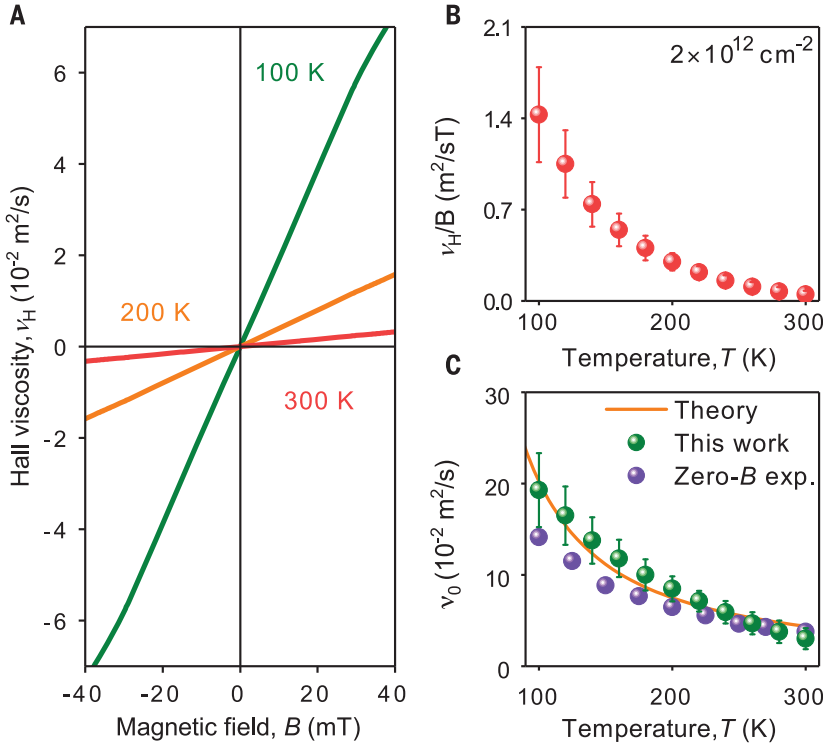

Fig. 3. Hall viscosity in graphene. (**A**) Examples of ν_H extracted by using data from Fig. 2A. (**B**) ν_H/B as a function of T. (**C**) Zero-field viscosity ν_0 extracted from our $R_A(B)$ measurements (green). Solid curve indicates theory (*11*). Purple symbols indicate previous experiments (*8*). For (A) to (C), MLG at $n = 2 \times 10^{12}$ cm^{-2}. No fitting parameters were used for the theory curve in (C). Error bars in (B) and (C) represent the scatter for measurements by using different L. The notable increase of the error below 150 K indicates that the electron system starts exiting the hydrodynamic regime (*7*, *12*).

induces ϕ of the opposite polarity with respect to those causing the B shifts in R_v. Indeed, the vicinity curve in Fig. 1F is shifted, for example, upward for hole doping and positive B, whereas the ordinary HE would shift it downward [(*22*), section 6]. This behavior agrees well with the opposite signs of the contributions expected from V_H and ν_H toward R_v, as shown in theoretical Fig. 1, C and D.

For further analysis, we define the Hall (odd) component of the vicinity resistance as $R_A(B) = [R_v(B) - R_v(-B)]/2$. The antisymmetrization removes the contributions that are symmetric in B and caused by the longitudinal viscosity ν and the Ohmic flow (*6*, *16*). Examples of the $R_A(B)$ curves for MLG and BLG devices are shown in Fig. 2A and fig. S3A, respectively. Within the ranges of T and B used in our experiment, the dependences are linear in B for all the studied devices and for all L. By analogy with the conventional Hall coefficient, where $\alpha_H = R_H ne/B \equiv 1$, it is instructive to introduce the viscous Hall coefficient, $\alpha_{VH} = R_A ne/B$ (*22*). In this form, the antisymmetric contribution R_A is effectively normalized by the ordinary HE, which provides a sense of the magnitude for the observed viscous effects.

Shown in Fig. 2B is the T dependence of α_{VH} obtained by using data such as those in Fig. 2A. Above 100 K, at which the hydrodynamic regime becomes fully developed (*6*, *7*, *10*, *12*), the viscous contribution reaches 20% of the ordinary HE and has the opposite sign (Fig. 2B). $|\alpha_{VH}|$ decreases with increasing T and eventually disappears below noise above room T. This T dependence was found to be universal for all the studied devices (fig. S2C). The observed behavior is detailed in Fig. 2, D and E, by plotting $\alpha_{VH}(T, n)$ for MLG and BLG. The maps are somewhat different because of different viscosities of the two graphene systems (*6*, *10*, *11*) but show similar trends as functions of n and T. We have also studied how α_{VH} depends on L and found that it decreases with increasing L, practically disappearing if the voltage probe is placed further than ~2 μm from the current-injecting contact (Fig. 2C). The latter highlights the importance of the vicinity geometry to detect viscous effects.

The anomalous viscous contribution to the HE, which is found by using the vicinity geometry, is fully consistent with our measurements of a local Hall resistance [(*22*), section 6]. To this end, we again used voltage contacts close to the current injector (for example, using $R_{35,16}$) and compared those measurements with the standard HE geometry ($R_{42,16} \equiv R_{16,42}$). The latter exhibited the ordinary HE with $\alpha_H = 1$, as expected. By contrast, the local Hall resistance was notably suppressed in the hydrodynamic regime (fig. S6) and agreed quantitatively with the behavior of α_{VH} reported above.

Here, we turn to theory. In the linear-response and steady-state regimes, 2D viscous transport in the presence of a perpendicular field B (in the z direction) is described by the Navier-Stokes equation

$$\frac{\sigma_0}{ne}\nabla\phi(\boldsymbol{r}) = (1 - D_v^2\nabla^2)\boldsymbol{v}(\boldsymbol{r}) + \omega_c\tau(1 + D_H^2\nabla^2)\boldsymbol{v}(\boldsymbol{r}) \times \hat{\boldsymbol{z}} \quad (1)$$

in conjunction with the continuity equation and no-slip boundary conditions (*16*, *22*). Here, $\boldsymbol{v}(\boldsymbol{r})$ is the local fluid velocity, $\omega_c = eB/m$ is the cyclotron frequency for electrons with the effective mass m, $\sigma_0 = ne^2\tau/m$ is the Drude conductivity, and τ is the transport time with respect to momentum-nonconserving collisions, such as scattering on phonons. The right-hand side of Eq. 1 contains two terms. The first describes the electric current and viscous friction parameterized through the diffusion constant, $D_v = \sqrt{\nu\tau}$. The second term arises from the Lorentz force $\boldsymbol{F}_L = -(\omega_c m)\boldsymbol{v}(\boldsymbol{r}) \times \hat{\boldsymbol{z}}$ and its viscous counterpart that depends on ν_H and is parameterized through another diffusion constant, $D_H = \sqrt{\nu_H/\omega_c}$. The Hall friction acts against $\boldsymbol{F}_L$, which also means that ν_H does not perform any work on the electron fluid and, therefore, is a dissipationless coefficient.

For the half-plane geometry (fair approximation for our devices) and close to the injection point, the above equation can be solved analytically (*16*), yielding $\phi(\boldsymbol{r})$ shown in Fig. 1, A to D (examples of the potential and current maps calculated taking into account the finite device width are provided in fig. S4). The Hall contribution to the vicinity resistance can be written as

$$R_A = -\sigma_0^{-1}\xi\left(\frac{L}{D_v}\right)\frac{\nu_H}{\nu} \quad (2)$$

where $\xi(x) = [L_1(x) - I_1(x)]/2x$, and $L_1(x)$ and $I_1(x)$ are the modified Struve and Bessel functions, respectively (*16*). The function $\xi(L/D_v)$ decreases monotonically with increasing L, behaving as $D_v/\pi L$ for $L \gg D_v$. The L dependence expected for our devices by using Eq. 2 is plotted in Fig. 2C, showing reasonable agreement with the experiment (especially in terms of the absolute values),

even without taking into account the finite width (~0.3 μm) of our current and voltage contacts.

The measured $R_A(B)$ such as shown in Fig. 2A can be used to extract v_H. To this end, we rewrite Eq. 2 as $\nu_H = -R_A\sigma_0\nu/\xi(L/\sqrt{\nu\tau})$, where σ_0 and τ can be deduced from standard longitudinal resistivity measurements (*6*, *8*). The longitudinal viscosity $\nu(B)$ can be approximated by using the semiclassical expression $\nu(B) = \nu_0 \frac{B_0^2}{B^2+B_0^2}$, where ν_0 is the kinematic viscosity in zero B, and $B_0 = \hbar v_F k_F/(8e\nu_0)$ is the characteristic magnetic field expressed through the Fermi wave number k_F, the Fermi velocity v_F, and the reduced Planck constant $\hbar$ (*16*, *24*, *25*). For the reported range of n and T, B_0 is much larger than the fields in our experiments. Accordingly, we can assume $\nu \approx \nu_0$ in Eq. 2 and then use ν_0 found experimentally in (*8*). Using the above protocol, it is straightforward to calculate ν_H and its B and T dependences. Examples are shown in Fig. 3, A and B. One can see that the Hall viscosity is linear in B and rapidly decreases with increasing T.

For consistency, we cross-checked the above analysis against the results obtained previously (*8*) for zero-field viscosity ν_0. To this end, the field dependence of $R_A = R_A[\nu_H(B), \nu(B)]$ originates from changes in both longitudinal and Hall viscosities. The full formula for $\nu(B)$ is given above, whereas the same semiclassical consideration (*16*, *24*) for the Hall viscosity yields $\nu_H(B) = \nu_0 \frac{BB_0}{B^2+B_0^2}$. This allows us to redefine the anomalous Hall contribution as $R_A[\nu_0, B]$ and calculate ν_0 from the measured $R_A(B)$ dependences, such as in Fig. 2A. ν_0 extracted by using this procedure is compared in Fig. 3C with the values found independently in (*8*). The figure shows good agreement between the two analyses and with the viscosity expected theoretically (*11*).

Last, the above hydrodynamic description is also consistent with the large negative magnetoresistance observed in our graphene devices at elevated T by using the standard longitudinal geometry (*22*). The magnetoresistance can be described accurately, without any fitting parameters (fig. S5), by using the same viscosity values as found experimentally in Fig. 3C. Similar magnetoresistance was reported in other high-quality 2D systems and attributed to ballistic transport affected by electron-electron interactions (*26*, *27*). Only recently has it been realized that the anomalous negative magnetoresistance at elevated T may signify the presence of a viscous flow and can also be described by the hydrodynamic approach (*15*, *24*), which is consistent with our work (*22*). It would be interesting to expand studies of the Hall viscosity into the quantum HE regime, which attracts considerable theory interest (*28*–*30*), but unfortunately, no experimental procedure has so far been suggested to probe this regime.

REFERENCES AND NOTES

1. R. N. Gurzhi, *Sov. Phys. Usp.* **11**, 255–270 (1968).
2. M. J. M. de Jong, L. W. Molenkamp, *Phys. Rev. B* **51**, 13389–13402 (1995).
3. A. O. Govorov, J. J. Heremans, *Phys. Rev. Lett.* **92**, 026803 (2004).
4. P. J. W. Moll, P. Kushwaha, N. Nandi, B. Schmidt, A. P. Mackenzie, *Science* **351**, 1061–1064 (2016).
5. J. Gooth *et al*., *Nat. Commun.* **9**, 4093 (2018).
6. D. A. Bandurin *et al*., *Science* **351**, 1055–1058 (2016).
7. D. A. Bandurin *et al*., *Nat. Commun.* **9**, 4533 (2018).
8. R. Krishna Kumar *et al*., *Nat. Phys.* **13**, 1182–1185 (2017).
9. A. Lucas, K. C. Fong, *J. Phys. Condens. Matter* **30**, 053001 (2018).
10. D. Y. H. Ho, I. Yudhistira, N. Chakraborty, S. Adam, *Phys. Rev. B* **97**, 121404 (2018).
11. A. Principi, G. Vignale, M. Carrega, M. Polini, *Phys. Rev. B* **93**, 125410 (2016).
12. A. Shytov, J. F. Kong, G. Falkovich, L. Levitov, *Phys. Rev. Lett.* **121**, 176805 (2018).
13. J. Crossno *et al*., *Science* **351**, 1058–1061 (2016).
14. J. E. Avron, *J. Stat. Phys.* **92**, 543–557 (1998).
15. T. Scaffidi, N. Nandi, B. Schmidt, A. P. Mackenzie, J. E. Moore, *Phys. Rev. Lett.* **118**, 226601 (2017).
16. F. M. D. Pellegrino, I. Torre, M. Polini, *Phys. Rev. B* **96**, 195401 (2017).
17. L. V. Delacrétaz, A. Gromov, *Phys. Rev. Lett.* **119**, 226602 (2017).
18. I. Torre, A. Tomadin, A. K. Geim, M. Polini, *Phys. Rev. B* **92**, 165433 (2015).
19. L. Levitov, G. Falkovich, *Nat. Phys.* **12**, 672–676 (2016).
20. G. Falkovich, L. Levitov, *Phys. Rev. Lett.* **119**, 066601 (2017).
21. F. M. D. Pellegrino, I. Torre, A. K. Geim, M. Polini, *Phys. Rev. B* **94**, 155414 (2016).
22. Materials and methods are available as supplementary materials.
23. C. W. J. Beenakker, H. van Houten, *Solid State Phys.* **44**, 1–228 (1991).
24. P. S. Alekseev, *Phys. Rev. Lett.* **117**, 166601 (2016).
25. M. S. Steinberg, *Phys. Rev.* **109**, 1486–1492 (1958).
26. Q. Shi *et al*., *Phys. Rev. B* **89**, 201301 (2014).
27. V. T. Renard *et al*., *Phys. Rev. Lett.* **100**, 186801 (2008).
28. J. E. Avron, R. Seiler, P. G. Zograf, *Phys. Rev. Lett.* **75**, 697–700 (1995).
29. I. V. Tokatly, G. Vignale, *Phys. Rev. B* **76**, 161305 (2007).
30. F. D. M. Haldane, *Phys. Rev. Lett.* **107**, 116801 (2011).
31. A. I. Berdyugin *et al*., Measuring Hall viscosity of graphene's electron fluid. Zenodo (2019); doi:10.5281/zenodo.2562181.

ACKNOWLEDGMENTS

Funding: This work was supported by the European Research Council, the Graphene Flagship, and Lloyd's Register Foundation. D.A.B. acknowledges the financial support from Leverhulme Trust, and R.K.K. acknowledges that from the EPSRC. **Author contributions:** D.A.B. and A.K.G. designed and supervised the project. A.I.B. and D.A.B. performed electrical measurements. S.G.X. and M.B.S. fabricated devices. A.I.B. and D.A.B. analyzed the data with input from R.K.K. and A.K.G.; F.M.D.P., A.P., I.T., and M.P. provided theoretical support. T.T. and K.W. provided hBN crystals. D.A.B. and A.I.B. wrote the manuscript with help from A.K.G. All the authors contributed to discussions. **Competing interests:** The authors declare no competing interests. **Data and materials availability:** The data reported in this work are archived at Zenodo (*31*).

SUPPLEMENTARY MATERIALS

www.sciencemag.org/content/364/6436/162/suppl/DC1
Supplementary Text
Figs. S1 to S6
References (*32*–*40*)

4 May 2018; accepted 19 February 2019
Published online 28 February 2019
10.1126/science.aau0685

Measuring Hall viscosity of graphene's electron fluid

A. I. Berdyugin, S. G. Xu, F. M. D. Pellegrino, R. Krishna Kumar, A. Principi, I. Torre, M. Ben Shalom, T. Taniguchi, K. Watanabe, I. V. Grigorieva, M. Polini, A. K. Geim and D. A. Bandurin

Science **364** (6436), 162-165.
DOI: 10.1126/science.aau0685originally published online February 28, 2019

Electron hydrodynamics in graphene

Electrons can move through graphene in a manner reminiscent of fluids, if the conditions are right. Two groups studied the nature of this hydrodynamic flow in different regimes (see the Perspective by Lucas). Gallagher *et al.* measured optical conductivity using a waveguide-based setup, revealing signatures of quantum criticality near the charge neutrality point. Berdyugin *et al.* focused on electron transport in the presence of a magnetic field and measured a counterintuitive contribution to the Hall response that stems from hydrodynamic flow.

Science, this issue p. 158, p. 162; see also p. 125